JOURNAL OF CATALYSIS 71, 411–422 (1981)

Surface Enrichment of Pt–Rh Alloy Particles by Oxidation–Reduction Cycling[1]

T. WANG AND L. D. SCHMIDT

Department of Chemical Engineering and Materials Science, University of Minnesota, Minneapolis, Minnesota 55455

Received May 8, 1981; revised July 7, 1981

X-Ray photoelectron spectroscopy (XPS) is used to examine the surface composition of 50 to 200-Å Pt, Rh, and Pt–Rh particles on planar amorphous SiO_2 following heat treatment at various temperatures in air or H_2. It has been shown previously by transmission electron microscopy that this treatment produces an expansion of oxidized particles parallel to the surface and the splitting of particles upon reduction. In this study, the composition of the surface layer is measured directly by examining the Rh, Pt, and O XPS signals from the particles. It is found that for a 50–50 alloy the Rh/Pt ratio increases by a factor of at least 3 upon oxidation and that the ratio remains above 2 upon heating in H_2 to above 500°C. Surface oxidation of Rh can be detected in both Rh and O signals just above room temperature, while much higher temperatures are required for oxides to be detected by electron diffraction. The enhanced Rh signal persists to much higher temperature for composition near 50% Pt than for either excess Rh or excess Pt. Oxidation–reduction cycling can produce nonequilibrium surface compositions for any alloy systems in which only one species is oxidized, and this configuration may be retained in the catalyst at temperatures below those where bulk diffusion of metal occurs. Other compound formation and decomposition cycles could be used to prepare enriched surfaces for many catalyst systems.

INTRODUCTION

Supported alloy catalysts are frequently found to possess many desirable properties over the individual metals. This has been suggested to arise from electronic properties of the alloys, the different types of sites on alloys, and various types of deactivation resistances of alloys (*1, 2*). As examples, Pt–Re and Pt–Ir particles offer higher selectivity and greater coke resistance in reforming than does Pt alone (*3–6*), Co–Mo catalysts are more poison resistant in hydrodesulfurization (*7*), and Pt–Rh has superior properties to the individual metals in NO removal in the automotive converter and in NH_3 oxidation to NO in HNO_3 production (*8, 9*).

We have recently shown from scanning transmission electron microscopy (STEM) studies of a number of alloys of Pt, Pd, Rh, and Ir on SiO_2 and Al_2O_3 that heat treatment in air followed by reduction in H_2 produces quite different morphologies than does heat treatment under vacuum or in an inert atmosphere (*10–14*). This can produce segregation of particles into individual components, spreading of particles parallel to the surface, and redispersion of particles into smaller ones.

Figure 1 summarizes TEM results for 52% Rh–48% Pt alloy on amorphous SiO_2. The micrographs are of the same particles following heat treatment for 1 h at a pressure of 1 atm of air or H_2 at the temperatures indicated. Figure 1a shows the original alloy particles and Fig. 1b the alloy after oxidation at 600°C to form Rh_2O_3 as shown by electron diffraction. Figures 1c–f show effects of heating in H_2 at 25, 150, 500, and 700°C, respectively. At 150°C all Rh_2O_3 is reduced to metal, but even at 500°C all

[1] This work was partially supported by the Petroleum Research Foundation under Grant 10864-AC7, and by the National Science Foundation under Grant CPE 8017440. XPS analysis was obtained using the NSF Regional Instrumentation Facility for Surface Analysis at the University of Minnesota.

0021-9517/81/100411-12$02.00/0

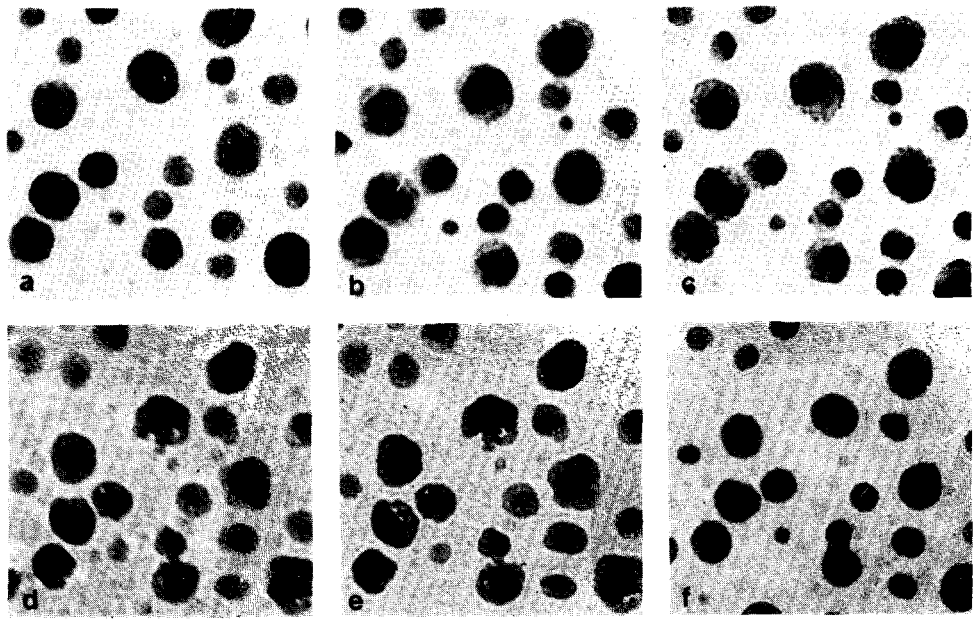

FIG. 1. Transmission electron micrographs showing the morphologies of 52% Rh–48% Pt alloy particles on SiO_2 illustrating segregation and splitting of alloy particles. The sample was heated sequentially (a) in H_2 at 650°C, (b) in air at 600°C, and then reduced in H_2 at (c) 25°C, (d) 150°C, (e) 500°C, and (f) 700°C, each for 1 h. Micrograph (c) shows tiny Rh crystallites while (d) and (e) indicate dark cores of Pt and lighter shells of Rh.

particles exhibit high-contrast cores and lighter shells. At 700°C particles have again become homogenized.

These TEM results strongly suggest that oxidation and reduction cycling is capable of producing different compositions on the particle surfaces which should have a strong influence on catalytic properties. However, microscopy alone does not provide surface information.

X-Ray photoelectron spectroscopy (XPS) is capable of probing the composition and chemical state of atoms in the top 5–10 Å of a surface, although for supported metals the sensitivity for small metal loadings has made quantitative analysis difficult. Porous pellet supports must also be pulverized or examined on their external surfaces, and this causes further complications in interpretation of XPS results (*15*). However, XPS has been used extensively to study many catalysts systems such as Co–Mo on Al_2O_3 hydrodesulfurization catalysts (*16–18*), copper aluminate catalysts (*19*), NiO on Al_2O_3 and SiO_2 (*20*), and platinum metals on various supports (*21–26*). Pt cannot be studied on Al_2O_3 by XPS because its major peak overlaps the major Al peak. Rh has been studied most extensively on carbon by Brinen *et al.* (*25–26*) who followed its oxidation from the chemical shift of the Rh 3*d* lines.

In this paper we examine Pt–Rh alloy particles on SiO_2 using XPS following heat treatment in H_2 or air. This study examines the same or identical particles as those which were used in previous TEM examination of that system. Thus, the present XPS results can be directly correlated with morphologies.

EXPERIMENTAL

Measurements were made on 50 to 200-Å-diameter particles of Pt–Rh and individual metals on planar amorphous SiO_2 (*10–14*). The SiO_2 was prepared by air oxidizing a 1-cm disk of high-purity Si to obtain a 1000-Å-thick layer of amorphous SiO_2 on

its surface. Then 10 to 20-Å films of Pt and Rh were vacuum deposited sequentially and heated in H_2 to form metal particles. The properties of the surface and particles were determined by TEM using a specimen on which a 500-Å-thick Si flake was placed over a hole in the Si disk. Air oxidation at 1200°C followed by metal deposition and heating in H_2 at 600°C produces complete oxidation of SiO_2 and forms metal particles of the desired size. In some experiments the same specimens were examined by XPS and TEM, but most specimens were merely prepared by identical methods.

Specimens were heated in flowing air or H_2 for 1 h at temperatures indicated and allowed to cool to room temperature before removal. In all experiments the same sample was transferred repeatedly between the furnace and the XPS system for treatment and analysis. Most results shown were repeated on several specimens with good reproducibility between specimens.

X-Ray photoelectron spectra were obtained on a Perkin–Elmer physical electronics model 555 system with a Mg$K\alpha$ anode ($h\nu$ = 1253.6 eV). Peak positions were always within 1 eV of tabulated positions, presumably because the high electrical conductivity of the Si core of the specimen minimized charging. Peak energies were determined relative to the Si (103.4 eV) and C (284.6 eV) peaks on the specimen. Typical survey scans required 3 min and high-resolution scans of Rh, Pt, and O peaks required 30 to 60 min for a peak resolution of ~1.3 eV. Peak positions of these elements were reproducible to within ±0.1 eV on all specimens examined.

The substrate before metal deposition showed only Si and O peaks in XPS and AES except for small amounts of carbon which were estimated to be much less than a monolayer. Deposition of metals also produced no detectable contaminants. Relative amounts of Pt and Rh were determined from weight losses of evaporation sources, and compositions are regarded as accurate to within a few percent. For H_2-treated particles the Pt/Rh ratios agreed very well with published XPS sensitivities of these metals. Data are displayed as surface atomic ratios obtained from these calibrations by measuring peak areas. For relative concentrations in various chemical states, curves were fit using Gaussian peaks with the experimental resolution.

RESULTS

Figure 2 shows typical XPS survey spectra of a 50% Pt–Rh alloy. Figure 2a is the initial film with 10 Å of Pt deposited on top of 10 Å of Rh. Figure 2b shows the same specimen after heating to 600°C in H_2 to

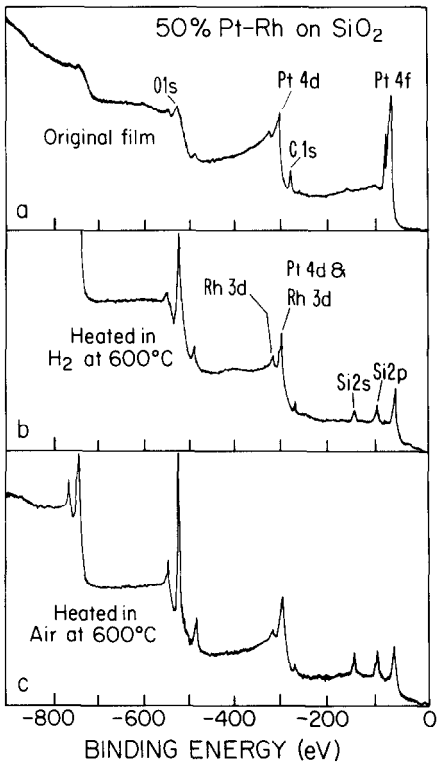

FIG. 2. Typical XPS survey spectra of a silica-supported 50% Pt–50% Rh alloy sample. (a) is the initial film with 10 Å of Pt deposited on top of 10 Å of Rh, while (b) and (c) show the spectra of the same specimen after heating to 600°C in H_2 and air, respectively. The 20 Å of metal completely buries the substrate and 10 Å of Pt nearly buries the Rh. This indicates that the XPS depth sensitivity in these experiments is ~10 Å.

break up the film into alloy particles, and Fig. 2c shows this specimen after heating in air at 600°C.

The successively deposited Rh and Pt film shows no Si peaks, only small Rh peaks, and predominantly Pt with traces of O and C. This indicates that 20 Å of metal completely buries the substrate Si and that 10 Å of Pt nearly buries the Rh. Thus, the depth sensitivity of XPS is confirmed to be approximately 10 Å, and the films deposited at 25°C are confirmed to be continuous (as shown also by TEM) (*12*). Thus, the mean escape depth of XPS electrons is observed to be ~10 Å. This is somewhat smaller than that typically observed from metals and may result partially from low backscattering of these electrons from the low-atomic-number SiO_2 substrate.

The Rh 3*d* and Pt 4*d* lines overlap, so compositions of alloys were determined from the Rh $3p_{3/2}$ at 498 eV and the Pt 4*f* at 71 and 74.5 eV. Silicon, oxygen, and carbon lines exhibit no interferences with these elements, and peaks are seen to be large enough to obtain detailed peak position, area, and shape analysis of all elements.

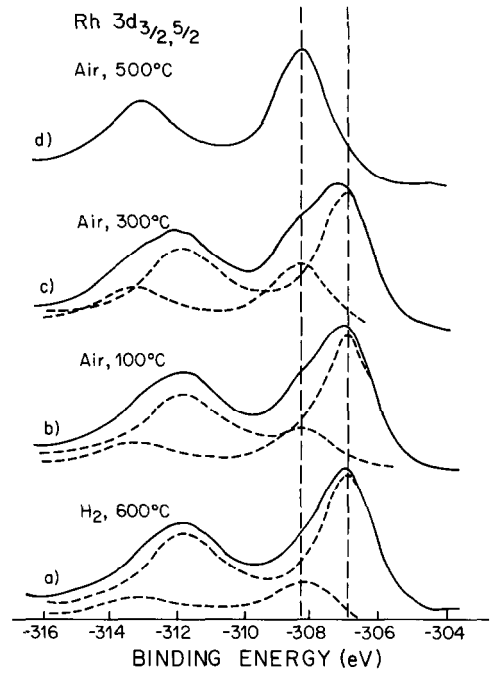

FIG. 3. High-resolution XPS spectra of the Rh 3*d* doublet from Rh particles supported on SiO_2. Spectra were obtained after treatment sequentially (a) in H_2 at 600°C, (b) in air at 100°C, (c) in air at 300°C, and (d) in air at 500°C. High-binding-energy peaks at 308.2 and 313.2 eV indicate Rh^{3+} from Rh_2O_3. Broken curves represent fits to data with experimental peaks from Rh metal and Rh_2O_3.

Rh on SiO_2

Figures 3 and 4 show high-resolution scans of Rh 3*d* and O 1*s* peaks for a succession of heat and gas treatments going from bottom to top in each figure. Heating in H_2 at 600°C produces predominantly metallic Rh with peaks at 307.0 and 311.8 eV, in good agreement with literature values (*27*) and with spectra of Rh foils obtained in this laboratory.

Small shoulders at higher binding energies of 308.2 and 313.2 eV are evident in Fig. 3b. These were confirmed to be Rh^{3+} by comparing with Rh_2O_3 powder on a gold foil. Upon heating at successively higher temperatures of 100, 300, and 500°C, the oxide peaks increase and metal peaks decrease until at 500°C only Rh^{3+} peaks remain. Broken curves in Fig. 3 represent fits to data with experimental peaks from Rh metal and oxide.

The O 1*s* region is shown in Fig. 4, which indicates a succession of heat treatments of a single sample for 1 h in gases at 1 atm at temperatures shown. The oxygen from SiO_2 occurs at 532.6 eV, while the peak at 530 eV is due to Rh_2O_3. Both Rh and O signals indicate that some Rh_2O_3 is formed even at room temperature, probably upon transfer of the sample in air to the XPS chamber. Oxidation is seen to produce Rh_2O_3 at the surface even at 300°C, while electron diffraction detects only Rh metal (no Rh_2O_3) until the specimen had been heated to ~500°C.

Figure 4 shows that treatment of Rh_2O_3 particles in H_2 at 150°C produces complete reduction to Rh metal. Electron diffraction also indicates the absence of Rh_2O_3 in H_2 at

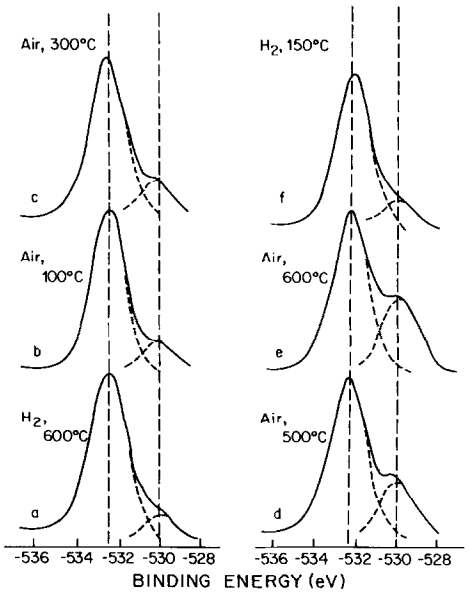

FIG. 4. XPS spectra of the O 1*s* level from a sample of Rh supported on SiO_2. The sample was heated sequentially (a) in H_2 at 600°C, (b) in air at 100°C, (c) in air at 300°C, (d) in air 500°C, (e) in air 600°C, and (f) in H_2 at 150°C. Treatment of Rh_2O_3 particles in H_2 at 150°C produces complete reduction to Rh metal.

150°C, but the diffraction lines of Rh metal are barely visible; this was interpreted (*14*) as suggesting that either crystals are very small or the reduced Rh metal is amorphous. However, XPS shows that treatment in H_2 at 150°C produces only Rh metal.

These and other data were analyzed quantitatively as shown in Fig. 5. The ordinate is element atomic ratio using tabulated XPS sensitivity calibrations of Rh, O, and Si. The points on the abscissa indicate successive treatments at 1 atm in air or H_2 for 1 h at temperatures indicated. The Rh/Si ratio increases upon treatment in air and decreases upon treatment in H_2 as does the O/Si ratio. However, the 530.0-eV O peak exhibits a large increase upon oxidation and nearly disappears upon reduction. The 532.6-eV peak is unchanged from any gas or temperature treatment as expected since it represents the O/Si ratio of SiO_2 (measured here to be ~2.5).

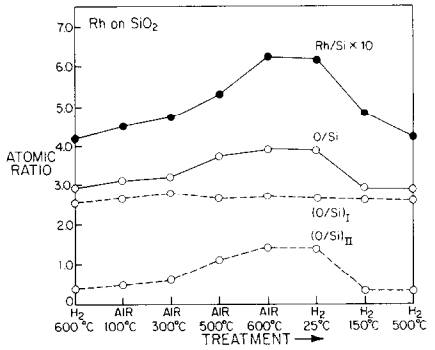

FIG. 5. Plot of XPS peak areas, shown as the ratio of O/Si and Rh/Si, alloy functions of treatment from the data of Figs. 3 and 4. $(O/Si)_I$ and $(O/Si)_{II}$ represent the atomic ratios of O/Si from SiO_2 and Rh_2O_3 after deconvolution. Both Rh/Si and O/Si ratios increase upon treatment in air and decrease upon treatment in H_2.

Pt on SiO_2

Figure 6 shows O/Si and Pt/Si peak ratios following heat treatments for pure Pt on SiO_2, similar to those just described for Rh on SiO_2. The O/Si ratio remains unchanged for all treatments, and no O peaks except that at 532.6 eV were noted.

The Pt/Si ratio from the original film drops sharply upon heating in H_2 at 600°C as the film breaks up into Pt particles. Continued treatment in air produces no change in Pt/Si until 700°C where the Pt signal falls significantly. The irreversible decrease above 600°C is caused by sintering

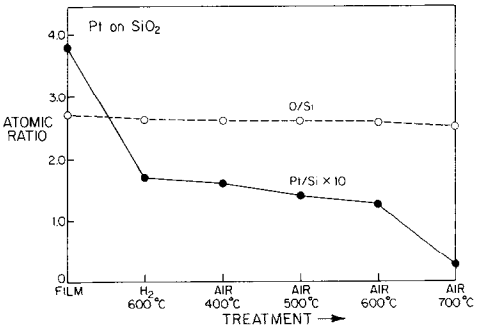

FIG. 6. Atomic ratios of O/Si and Pt/Si following treatment of pure Pt on SiO_2. The O/Si ratio remains unchanged for all treatments while the Pt/Si signal falls irreversibly upon heating in air at 700°C.

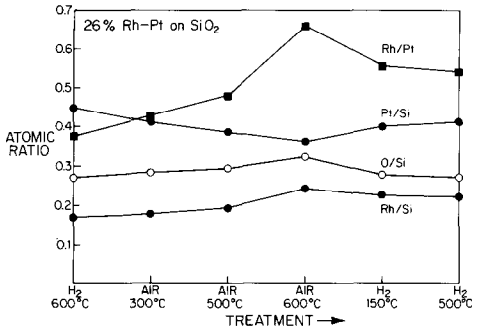

FIG. 7. Atomic ratios metal/Si, O/Si, and Rh/Pt obtained from XPS peak areas of a 26% Rh–74% Pt alloy sample as functions of treatment. The amounts of metals were determined from the Rh $3p_{3/2}$ and Pt $4f$ XPS signals.

of Pt particles and volatilization into PtO_2 which leaves the specimen (*10*).

We find no evidence from XPS for solid oxide formation upon heating Pt particles in air. This is in agreement with TEM electron diffraction which should detect only bulk phases but is in disagreement with EXAFS which yields evidence for Pt–O bond distance (*28*).

Rh–Pt Alloys

Figures 7 and 8 show Pt–Rh alloys with 26 and 73% Rh, respectively. The Rh/Si ratio increases upon O_2 treatment and decreases upon H_2 treatment, just as it does for Rh alone on SiO_2. However, when plotted as the Rh/Pt ratio, even larger change is evident upon oxidation. The Rh signal evidently increases and the Pt signal decreases upon treatment in air to 600°C. Note also that following these treatments Pt alone exhibits no change in the Pt/Si ratio, Fig. 6.

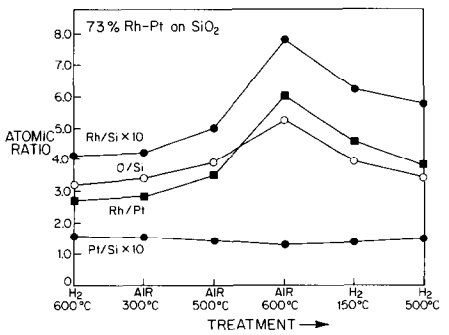

FIG. 8. Atomic ratios metal/Si, O/Si, and Rh/Pt obtained from XPS peak areas of a 73% Rh–27% Pt alloy sample as functions of treatment.

Treatment in H_2 does not produce an immediate decrease in Rh/Si upon decomposition of Rh_2O_3; at 150°C and even at 500°C the Rh/Pt ratios remain above the values they had upon initial particle formation.

The effect of oxidation and reduction is even more dramatic for the 48% Rh–Pt alloy, Fig. 9. At 600°C in air, the Rh/Pt ratio increases by a factor of ~3, with the largest increase between 550 and 600°C. Treatment in H_2 produces a decrease in the Rh/Pt ratio, but it remains at ~2 until 700°C where the alloy appears to return to its initial composition.

Sputter Depth Profiles

These results show that oxidation produces a Rh_2O_3 shell over the alloy particle which persists upon reduction. The thickness of these layers is obviously important in determining their properties and stability.

We used sputter depth profiling with XPS detection to estimate layer thicknesses. For these experiments several alloy specimens with 48% Rh were prepared identically (simultaneously) and then subjected to various gas and heat treatments. Since layers are less than 100 Å thick, low sputter rates over large sample areas were used. XPS spectra were obtained as a function of sputter time, and Pt/Si and Rh/Si ratios were determined. Experiments are, of course, destructive since the surface layer is removed by sputtering.

Figure 10a shows the original layer film with 10 Å of Pt on the surface and 10 Å of Rh underneath. The major peak is from Pt (see Fig. 2a) as expected. Sputtering for 20 min produces approximately equal Pt and Rh signals which both decay as more material is removed. The air-oxidized alloy, Fig. 10b, shows an excess of Rh (Rh/Pt ~3)

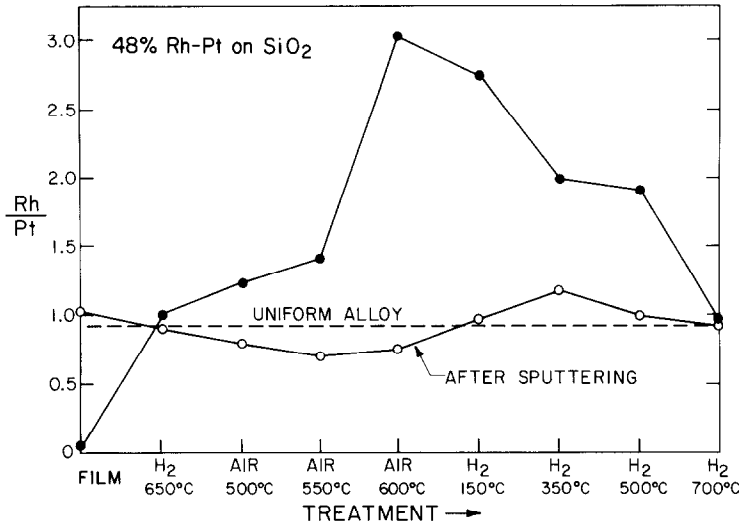

FIG. 9. Atomic ratio Rh/Pt obtained from XPS peak areas of the surface relative to the bulk ratio as function of treatment for a 48% Rh–52% Pt alloy. The Rh/Pt ratio increases by a factor of 3 upon oxidation and remains above 2 upon heating in H_2 to above 500°C. The broken line represents the surface composition of Rh and Pt after 1 h sputtering.

which persists to ~40 min, after which the surface have an excess of Pt. This surface is initially that of Fig. 9, and its complete spectrum is shown in Fig. 2b. The reduced

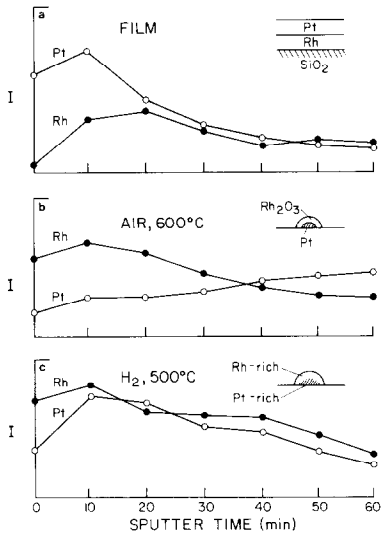

FIG. 10. Argon ion sputter depth profile for a 48% Rh–52% Pt alloy. (a) shows the original layered film with 10 Å of Pt on the surface and 10 Å of Rh underneath, while (b) and (c) show the profile after heating samples with the same composition in air to 600°C and in H_2 to 500°C, respectively. The sputtering rate was about 1 Å/min.

oxide, Fig. 10c, exhibits Rh enrichment initially, but within 10 min the Rh/Pt ratio becomes nearly unity and remains so until most metal has been sputtered away.

If we assume that sputtering removes ~1 Å/min (roughly calibrated from the film of Fig. 10a), then we estimate the Rh_2O_3 film to be ~30 Å thick. The enriched Rh layer after reduction is then only ~5 Å thick.

The data indicated by open circles in Fig. 9 are the Rh/Pt ratio after sputtering for approximately 1 h. The composition is seen to be nearly that of the bulk alloy. These experiments obviously give only qualitative depth-composition profiles because of many factors, especially the topography of the small alloy and oxide particles. However, after the Rh-enriched layer has been removed, the exposed surface has more Pt as expected. A total of nine identical alloy samples were prepared in these experiments and each was treated under conditions shown in Fig. 10. Results were consistent with those shown here, all indicating more Pt after the surface had been sputtered. This confirms that removal of the Rh cap on each particle exposes a core which is enriched in Pt. It also confirms that heat

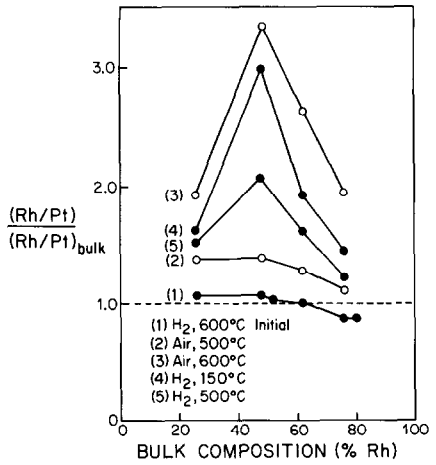

FIG. 11. Metal ratio Rh/Pt versus bulk alloy composition for different temperature and gas treatments. The segregation of Rh to the surfaces of particles due to oxidation is most pronounced near the 50%–50% Pt–Rh alloy.

treatments do not produce preferential evaporation of one metal.

DISCUSSION

Electron microscopy and XPS both show that surfaces of Pt–Rh alloy particles can be altered by oxidation–reduction cycling. One should expect that the surface of any metal or alloy catalyst particles can be altered by oxidation–reduction cycling. The surface area of a pure metal can be increased and for an alloy the surface can be enriched in the oxidizable species.

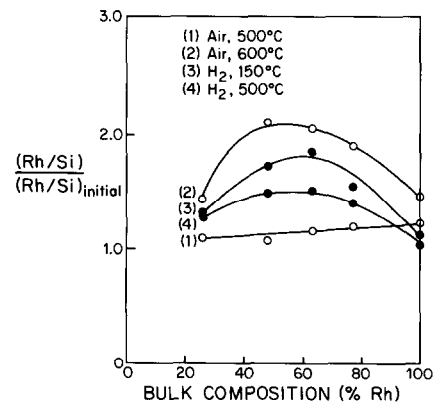

FIG. 12. Atomic ratio Rh/Si versus bulk alloy composition for temperature and gas treatments indicated.

Our results are summarized in Figs. 11 and 12, where the metal ratio Rh/Pt and the metal-to-support ratios, Rh/Si are plotted versus bulk alloy composition for different temperature and gas heat treatments.

An important aspect in utilization of these procedures in altering catalyst structures is the temperature stability of the structures formed, and in the next section the results will be summarized and interpreted in terms of processes involved. Interpretation of the XPS results depends sensitively on the calibration of atomic and depth sensitivities, and in the following section these will be discussed. Finally, these results suggest that chemical compound formation may be a general technique for altering catalyst structures, and in the last section these aspects will be considered.

Temperature Stability

For pure Rh, Figs. 5 and 12, the 50% increase in Rh/Si ratio upon oxidation is largely lost upon reduction, even at 150°C. TEM of this situation indicates that upon reduction the oxide particle breaks up at ~150°C into tiny metal crystallites whose geometric area is reduced from that of the original oxide. However, the stability of these particles is low, and by 300°C Rh crystallites have largely coalesced into the general shape and surface area of the original particles.

However, for alloys the enhanced Rh signal produced by oxygen treatment persists to much higher temperatures. Figures 11 and 12 show that even at 500°C the Rh/Pt ratio is above that of the original alloy. In the alloys the Rh/Si ratio also remains significantly above its initial value. Rhodium enrichment is most pronounced and most stable near the 50–50 alloy composition where a factor of 3 surface enhancement is produced by formation of Rh_2O_3, and even at 500°C the Rh/Pt ratio is ~2.

Three stages are evident upon heating the oxidized alloy particles. These stages and

their temperatures are summarized in Table 1 and Fig. 13. The first stage is reduction of Rh_2O_3 to Rh metal. This begins at room temperature and is complete by 100–150°C as measured by TEM and XPS. This leave 10 to 20-Å Rh crystallites on the SiO_2 and a shell of Rh metal ~20 Å thick over the Pt core of the particle. The second stage is the sintering or coalescence of the tiny Rh crystallites into the original particle. This occurs between 100 and 300°C to leave a single metal particle with Pt at its core and Rh at its periphery. The third stage is the homogenization of the segregated metal particle, and this does not occur until above 500°C.

Each stage should occur by a distinct process. Reduction is the chemical reaction

$$Rh_2O_3 + H_2 \rightarrow Rh + H_2O.$$

This highly exothermic process is limited by the reduction kinetics or by the diffusion of oxygen ions, H_2, or H_2O through Rh_2O_3 or metal. Sintering probably occurs by atomic diffusion (Ostwald ripening) of Rh atoms from the 10-Å crystallites to the parent particle. This is a surface diffusion process of Rh over itself or over SiO_2. Homogenization of the alloy requires interdiffusion of Rh and Pt within a particle. This is basically a bulk diffusion process.

The driving forces of these three stages are also quite different. Reduction is an irreversible reaction, and sintering is driven by the large surface energy difference between small particles and larger ones. However, homogenization within a particle is driven only by the entropy of mixing and the small difference in surface free energies of Rh and Pt. Tabulated values indicate that these are very similar (*29*), 1940 and 1865 ergs/cm², respectively.

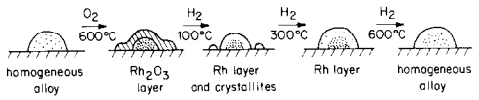

FIG. 13. Sketch of idealized alloy particle cross sections produced by oxidation–reduction cycling at temperatures indicated. These morphologies are determined from microscopy (Fig. 1) and by XPS (Figs. 7, 8, and 9).

Thus, the observation that reduction, sintering, and homogenization occur as distinct processes at quite different temperatures (100, 300, and 500°C) is consistent with the different transport paths and driving forces in each process: reduction being energetically favored and requiring little diffusion, and homogenization being driven mainly by the entropy of mixing and requiring bulk diffusion.

The surface and bulk diffusion paths of sintering and homogenization are in reasonable agreement with estimates of surface and bulk diffusion coefficients of Pt. The processes observed require motion of ~20 Å in ~1 h, and the random walk expression $X = (2Dt)^{1/2}$ requires that $D \geq 2 \times 10^{-17}$ cm²/sec to obtain either process. From extrapolation of the bulk diffusion coefficient of Pt this diffusion should occur at 700°C, while we observed mixing above

TABLE 1

Transformations in Alloy Particle Reduction

Stage	Process	Observed temperature (°C)	Path	Cause
I	Oxide reduction	25–150	Chemical reaction	Free energy of reaction
II	Metal Crystallite coalescence	100–300	Surface diffusion	Size dependence of surface energy
III	Composition homogenization	500–700	Bulk diffusion	Entropy of mixing

500°C and below 700°C. The surface diffusion coefficient of Pt has been reported to be 5×10^{-10} cm^2/sec at 600°C (*30*). This gives a temperature of ~200°C for the sintering process under the above conditions assuming an activation energy of 40 kcal/mole.

For pure Rh only stages I and II are possible, and this is consistent with the observation that Rh particles attain their original morphologies and surface compositions by ~300°C.

Surface Composition

In this section we shall comment on the surface sensitivity and accuracy of the XPS results. All ordinates in Figs. 5–9 are *atomic composition ratios* obtained from peak areas using published sensitivity calibrations (*27*). The Rh/Pt ratios are within a few percent of measured bulk compositions of the alloy particles for the hydrogen-annealed particles, and the metal/Si ratios are close to geometric areas of particle and SiO_2 exposed. Thus, we observe no large discrepancies between measured ratios and those expected for the simple situations. The values in fact suggest that composition ratios measured by XPS may be accurate to with ±10%.

As discussed previously, deposition of metals successively as films provides a direct calibration of the depth sensitivity of our XPS signals of ~10 Å. From Fig. 10 we obtain 20 and 5 Å as thickness of Rh_2O_3 and Rh layers on 50–50 alloy particles.

Corrections to sensitivities should be applied for relative densities of Rh in Rh_2 and in metal and for depth sensitivities in very thin layers. The Rh atom density ratio in metal and Rh_2O_3 is 1.5, and the sensitivity of the Rh XPS peak in the metal should be higher by this ratio. Also, for a very thin layer there should be some signal from the underlying Pt atoms, and this will reduce the Rh/Pt signal from its true surface value.

Both of these factors produce a measured Rh/Pt ratio which is *lower* than the true surface ratio. Thus, we conclude that the true Rh/Pt ratio upon oxidation and reduction of 50–50 alloy should be significantly greater than the measured ratio of ~3.

Surface Enrichment by Chemical Reaction Cycling

The process we describe is surface enrichment of an alloy by oxidation and then reduction. For a binary alloy AB where B forms a stable oxide BO but A does not, this process is

$$B + \tfrac{1}{2} O_2 \rightarrow BO$$

followed by

$$BO + H_2 \rightarrow B + H_2O,$$

with B (Rh) being transported to the surface in forming an oxide phase and being left there upon reduction. The necessary conditions for this process in an alloy are (1) one species must be oxidizable and the other not, and (2) the oxide must be reducible under conditions where diffusion of metal is sufficiently slow to prevent mixing upon reduction.

Many alloy combinations should be capable of exhibiting surface enrichment, although Pt and Au are the most inert metals. For bulk alloy foils, enrichment by this technique has been demonstrated for Pt–Rh (*31*), Pd–Au (*32*), Pd–Ag (*32*), Pt–Pd (*33*), and other binary alloys.

Wanger and others (*34*) have discussed the morphologies of alloys produced by oxidation, and these ideas suggest many possible configurations for oxidation and reduction of binary and ternary alloy catalysts under various conditions.

Other chemical reactions could of course be used to produce surface-enriched catalyst particles. Suppose B interacts with molecule X to form BX but A does not and that BS reacts with molecule X to form XY:

$$B + X \rightarrow BX$$

followed by

$$BX + Y \rightarrow B + XY.$$

Compounds such as sulfides, carbides, ni-

trites, chlorides, etc., could be formed from alloys then decomposed with gases such as O_2, H_2, CO, etc., to enrich alloy particles with one element of the alloy.

Chemical reaction cycling processes such as this are in principle capable of being used to produce surface enrichment of any species by finding a suitable compound formed by the element to be enriched. Formation and decomposition conditions must, of course, be suitable to trap the configuration formed under reaction conditions.

SUMMARY

Chemical reactions of catalyst particles with supports and with gases or liquids are the major processes by which catalysts are modified into desirable or undesirable configurations. We have shown that Pt–Rh alloy particles can be redispersed and surface enriched in Rh by oxidation–reduction cycling. All alloys with Pt except Au should produce similar behavior as long as the alloy forms a solid solution. Reaction cycling is much more powerful than annealing in an inert atmosphere because the driving forces are much larger (reaction free energies rather than surface free energies) and because the layers formed can be very thick and thus much more resistant to reversion to equilibrium configurations.

Segregation and enrichment should be expected for Pt alloys with Rh, Re, Ir, and Pd, although Pd may be sufficiently mobile to mix under any reasonable reaction temperatures. Re and Ir should be ideal candidates for surface enrichment because they are quite refractory and will diffuse only at very high temperatures.

Other reactions besides oxidation and reduction may be capable of yielding nonequilibrium surface compositions in cycling treatment processes. Such processes are probably operative in preparation and regeneration of many supported alloy catalyst systems. They may also be taking place in reactions with components in feedstocks to produce unintentional activation and deactivation of catalysts.

By stopping reduction at various temperatures, the transformations can be stopped at any of the stages listed in Table 1. This suggests additional possibilities for creating specific morphologies. For example, at Stage II the surface should consist of very small crystallites or amorphous phases. These surfaces can have high densities of high-index crystal planes, grain boundaries, and surface defects. We shall describe these morphologies and the effects of sulfiding in later papers.

REFERENCES

1. Anderson, J. R., "*Structure of Metallic Catalysts*." Academic Press, New York/London, 1975.
2. Ponec, V., *Catal. Rev.* **11**(1), 41 (1975).
3. Pollitzer, E. L., *Platinum Met. Rev.* **16**(2), 42 (1972).
4. Burch, R., *Platinum Met. Rev.* **22**(2), 57 (1978).
5. Sinfelt, J. H., U.S. Patent 3,953,368.
6. Rasser, J. C., "Platinum-Iridium Reforming Catalysts." Delft Univ. Press, Delft, 1977.
7. Schuit, G. C. A., and Gates, B. C., *AIChE J.* **19**, 417 (1973).
8. Schlatter, J. C., and Taylor, K. C., *J. Catal.* **49**, 42 (1977).
9. Taylor, K. C., and Schlatter, J. C., *J. Catal.* **63**, 53 (1980).
10. Chen, M., and Schmidt, L. D., *J. Catal.* **55**, 348 (1978).
11. Chen, M., and Schmidt, L. D., *J. Catal.* **56**, 198 (1978).
12. Chen, M., Wang, T., and Schmidt, L. D., *J. Catal.* **60**, 356 (1979).
13. Wang, T., and Schmidt, L. D., *J. Catal.* **66**, 301 (1980).
14. Wang, T., and Schmidt, L. D., *J. Catal.* **70**, 187 (1981).
15. Delgass, W. N., Hughes, T. R., and Fadley, C. S., *Catal. Rev.* **4**, 179 (1970).
16. Gajardo, P., Pirotte, D., Detosse, C., Grange, P., and Delmon, B., *J. Electron Spectrosc. Relat. Phenom.* **17**, 121 (1979).
17. Gajardo, P., Grange, C., and Delmon, B., *J. Catal.* **63**, 201 (1980).
18. Edmonds, T., and Mitchell, P. C. H., *J. Catal.* **64**, 491 (1980).
19. Ertl, G., Hierl, R., Knözinger, H., Thiele, N., and Urbach, H. P., *Appl. Surf. Sci.* **5**, 49 (1980).
20. Lorenz, P., Finster, J., and Wendt, G., *J. Electron Spectrosc. Relat. Phenom.* **16**, 267 (1979).

21. Scharpen, L. H., *J. Electron Spectrosc. Relat. Phenom.* **5,** 369 (1974).
22. Briggs, D., *J. Electron Spectrosc. Relat. Phenom.* **9,** 487 (1976).
23. Takasu, Y., Unwin, R., Tesche, B., and Bradshaw, A. M., *Surf. Sci.* **77,** 219 (1978).
24. Larking, F. P., Hughes, M. E., Anderson, J. R., and Foger, K., *J. Electron Spectrosc. Relat. Phenom.* **15,** 33 (1979).
25. Brinen, J. S., and Melera, A., *J. Phys. Chem.* **76,** 2525 (1972).
26. Brinen, J. S., Schmitt, J. L., Doughman, W. R., Achorn, P. J., Siegel, L. A., and Delgass, W. N., *J. Catal.* **40,** 295 (1975).
27. Mullenberg, G. E. (Ed.), "Handbook of X-ray Photoelectron Spectroscopy." Perkin–Elmer Press, 1978.
28. Via, G. H., Sinfelt, J. H., and Lytle, F. W., *J. Chem. Phys.* **71,** 690 (1979).
29. Weast, R. C., (Ed.), "Handbook of Chemistry and Physics," 58th ed. Chem. Rubber Co., Cleveland, Ohio, 1978.
30. Wynblatt, P., and Gjostein, N. A., *Prog. Solid State Chem.* **9,** 21 (1975).
31. Williams, F. L., and Nelson, G. C., *Appl. Surf. Sci.* **3,** 409 (1979).
32. Wood, B. J., and Wise, H., *Surf. Sci.* **52,** 151 (1975).
33. Kuijers, F. J., Teiman, B. M., and Ponec, V., *Surf. Sci.* **75,** 657 (1978).
34. Wanger, C., *J. Electrochem. Soc.* **99,** 369 (1952).